Energies **2013**, *6*, 6188-6210; doi:10.3390/en6126188

OPEN ACCESS

energies

ISSN 1996-1073

www.mdpi.com/journal/energies

Article

On the Efficacy of PCM to Shave Peak Temperature of Crystalline Photovoltaic Panels: An FDM Model and Field Validation

Valerio Lo Brano *, Giuseppina Ciulla, Antonio Piacentino and Fabio Cardona

Department of Energy, Information Engineering and Mathematical Models, DEIM, Viale delle Scienze, Ed.9, Palermo 90128, Italy; E-Mails: ina@dream.unipa.it (G.C.); piacentino@dream.unipa.it (A.P.); fabio.cardona@dream.unipa.it (F.C.)

* Author to whom correspondence should be addressed; E-Mail: lobrano@dream.unipa.it; Tel.: +39-091-2386-1918; Fax: +39-091-484-425.

Received: 12 July 2013; in revised form: 11 November 2013 / Accepted: 14 November 2013 / Published: 28 November 2013

Abstract: The exploitation of renewable energy sources and specifically photovoltaic (PV) devices have been showing significant growth; however, for a more effective development of this technology it is essential to have higher energy conversion performances. PV producers often declare a higher efficiency respect to real conditions and this deviation is mainly due to the difference between nominal and real temperature conditions of the PV. In order to improve the solar cell energy conversion efficiency many authors have proposed a methodology to keep the temperature of a PV system lower: a modified crystalline PV system built with a normal PV panel coupled with a Phase Change Material (PCM) heat storage device. In this paper a thermal model analysis of the crystalline PV-PCM system based on a theoretical study using finite difference approach is described. The authors developed an algorithm based on an explicit finite difference formulation of energy balance of the crystalline PV-PCM system. Two sets of recursive equations were developed for two types of spatial domains: a boundary domain and an internal domain. The reliability of the developed model is tested by a comparison with data coming from a test facility. The results of numerical simulations are in good agreement with experimental data.

Keywords: phase change material; crystalline photovoltaic modules; heat storage; finite difference method; experimental validation

Nomenclature:

A	is the surface of the control volume (m^2)
C	average heat capacity of an uncompressible substance (J/kg·K)
c_p	specific heat coefficient(J/kg·K)
f	liquid fraction
G	solar irradiance (W/m^2)
h	convective heat transfer coefficient ($W/m^2 \cdot K$)
h_{conv}	convective coefficients ($W/m^2 \cdot K$)
h_{rad}	radiative coefficients
I	total enthalpy (J/kg)
l	specific latent heat (J/kg)
L	latent heat component (J/kg)
n	position of the node (m)
P	net radiative power (W/m^2)
q	generic heat flux (W/m^2)
R	resistive electrical load (Ω)
S	sensible heat component (J/kg)
T	generic temperature; cell temperature of the PV panel (K)
T_{air}	external air temperature (K)
T_{sky}	sky temperature (K)
T_{PET}	temperature of the PET external surface of the PV panel (K)
T_{roof}	temperature of the external surface of the roof (K)
V	voltage generated by the PV panel (V)
$x = X(t)$	time function that identifies the position of the phase change boundary (m)
$\Delta x/2$	thickness of the superficial domain (m)
Δt	time step (s)
α	thermal diffusivity (m^2/s)
ε_{glass}	emissivity of the glass layer of the PV panel
ε_{PET}	emissivity of the PET external surface of the PV panel
λ	thermal conductivity (W/m·K)
σ	Boltzmann constant 5.67×10^{-8} ($W/m^2 \cdot K^4$)
τα	product of transmission coefficient of glazing and absorption coefficient of silicon

Subscripts:

i	initial time step
l	liquid phase
m	melting phase
s	solid phase
$p + 1$	present time interval
p	the previous time interval

t	current time step
$t + 1$	successive time step
0	superficial node

1. Introduction

The intense exploitation of fossil fuels has caused an increase in the concentration of carbon dioxide from 280 to 370 ppm and a consequent estimated global warming from 0.4 to 0.8 °C [1]. The global effort to fight the effects of global climate change has been oriented to reduce energy consumptions through new technologies [2] and to ensure a more efficient exploitation of Renewable Energy Sources (RES) [3].

Among RES, solar energy is the most important and available natural resource. During the last decade there was a widespread use of photovoltaic (PV) systems not only for decentralized production in advanced countries but also in developing countries, where the most likely alternative to produce electricity is related to the use of poor fuels (coal and lignite, peat, *etc*. which are very polluting) and biomass [4].

A key element of a wider dissemination of PV systems is represented by high power conversion efficiency. Concerning this point, the energy produced by a PV cell depends, apart from materials, on other two important parameters: the amount of the incident radiation and the temperature of the PV cell.

The performances of a PV panel in fact are defined by manufacturers according to the "peak power", which identifies the maximum electric power supplied by the PV panel when it receives an insolation of 1 kW/m^2 with air mass 1.5 and the cell temperature is maintained at 25 °C (Standard Test Conditions). These parameters are only observed under reference conditions, because solar radiation has a variable intensity and the panel is subjected to significant temperature variations, with temperature values much higher than 25 °C. In real conditions performances of a PV panel are different from those declared under the nominal conditions and the conversion efficiency decreases when the temperature of the cell increases [5].

The wind speed greatly influences heat exchange between the PV panel and the external environment, mitigating its temperature; however, the wind is often too weak, especially in densely populated urban areas [6–8], to provide the desirable cooling of the solar cell. Obviously, there are other parameters that can affect PV panel cooling [9,10]. Furthermore, releasing heat to the air in summertime will cause side effects like intensified heat islands in case of large numbers of installations.

Among other measures aimed to increase the energy conversion, Phase Change Materials (PCMs) have been receiving increased attention, due to their capacity to store large amounts of thermal energy in narrow temperature range. A PCM is a substance with a high heat of fusion which, by melting and solidifying at a certain temperature, is capable of storing and releasing large amounts of energy. Heat is absorbed or released when the material changes from solid to liquid and *vice versa*. PCMs represent a possible solution that may reduce peak loads and thermal energy consumption in buildings due to their good insulation properties and thermal inertia effects related to the phase change

phenomenon [11–13]. Despite the higher conductivity, compared to usual insulation materials used in buildings, PCM have been proved efficient in reducing peak heat fluxes by as much as 38% [14]. Indeed this property makes them ideal for passive heat storage in different building applications such as in the envelope of the building, in radiant floor heating systems, in free cooling systems, in photovoltaic elements and in building integrated PV [15–26].

The idea to couple the PCMs with the photovoltaic technology arises from the features of these materials to absorb large amounts of heat (keeping the temperature almost constant) when the heat is not required and overheating would cause a drop in the efficiency of photovoltaic cells. The absorbed heat should be then released to the surrounding air during night when the panel does not produce electrical power. The application of PCM coupled to a PV panel may represent an innovative technological solution to smooth daily temperature fluctuations and improve energy efficiency of the panel, however, PCMs are generally characterized by low thermal conductivity.

The capability of PCM to ensure a thermal regulation for a PV system can be better understood by analyzing heat transfer process across a multi-layered system in which one of the layers is composed by a material that changes phase during the day.

The aim pursued by the authors in this paper was to investigate a method to increase the energy performance of a photovoltaic panel by decreasing the operating temperature by means of PCM. This application has recently been suggested by other authors that have carried out some numerical studies. In this paper, a finite difference model capable of forecasting the variable temperature profile of a crystalline PV-PCM system is described; the adopted numerical scheme is presented in detail, also discussing the equations of the model and the resolution system using the FDM approach (finite difference method). In order to validate the numerical model, we performed a comparison with data derived by a real-time monitoring apparatus.

2. General Description of the PV-PCM Configuration

Considering a PV panel coupled with PCM system, the energy balance must take into account the presence of the phase-change material. Schematically, the energy exchanges in a crystalline PV-PCM system can be exemplified as shown in Figure 1.

Figure 1. PV-PCM cross-section (thicknesses not presented at real scale, for clarity of representation).

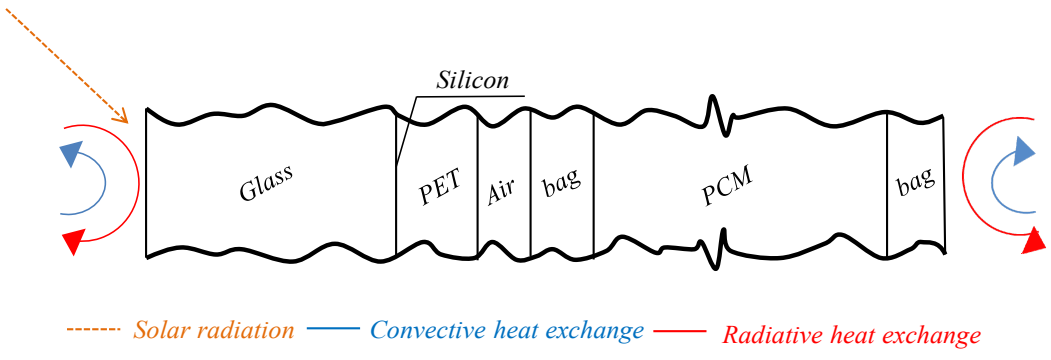

Due to the presence of a simple geometry, it was possible to adopt a one-dimensional approach, considering only a heat flow orthogonal to the PV plane. The simplification of the thermal problem,

compared to a more accurate representation in 2D or 3D [27], does not lead to unacceptable errors in the evaluation of the temperature field. The hypothesis of heat flow mono-dimensionality is in fact justified by ratio thickness/surface which is close to 0.02 m^{-1} in case of a crystalline PV-PCM system. The thermo-physical characteristics of each component are also constant in the other two directions and neglecting the effects relative to the edges of the panel, the overall energy balance remains practically unchanged. Furthermore the PCM is confined in small vacuum plastic bags of about 250 mL in volume. This configuration, because of high viscosity of the material in liquid phase, allows us to completely exclude the establishment of natural or buoyant convection. In Figure 1, h_{rad} and h_{conv} respectively represent the external radiative and convective coefficients.

Let us refer to a particular geometry, assuming the system composed by:

- A tempered glass sheet with a thickness of 3.2 mm (glass layer);
- 1 mm of PET plastic panel on which are "printed" the silicon cells; the silicon cells are considered having negligible thickness (plastic layer);
- An optional layer of air interposed between the panel and the heat storage system representing a possible imperfect contact (air layer);
- A plastic layer that takes into account the bag that contains the PCM (bag layer);
- About 5 cm of PCM (PCM layer).

Figure 1 represents the section of the geometry along the thickness of the crystalline PV-PCM system where it is possible to identify all the layers involved: the glass panel, the PET panel, the layer of air due to the imperfect contact of the envelope of PCM with the PV, the thickness of the envelope containing the PCM and the PCM layer itself.

The crystalline PV-PCM system is presented as a multi-layer plate exposed to solar radiation and exchanging heat with the external environment by convection and radiation. Depending on the properties of the PCM and on the amount of energy captured from the panel, the PCM layer can partially or totally melt during the maximum insolation, rejecting the same amount of energy initially stored (and possibly solidifying again) during the night. The first hypothesis considers the phase change perfectly isothermal. This hypothesis is not very far from reality because many PCMs are characterized by isothermal phase changes, while some paraffin and eutectic mixtures have a very short range of temperature during transition. However, the assumption of isothermal phase change represents a simplification of the real phenomenon where there are three phases: solid, mushy, and fluid [28,29]. In the following model proposed by the authors, an approach that takes into account the liquid fraction is adopted, neglecting the mushy phase. In case of non-isothermal transition, if the c_p value is known at any temperature; the problem is reduced to a heat conduction case.

2.1. Energy Balance of PV System

In order to evaluate the energy production of the PV panel and the resulting radiative and convective exchanges with surrounding environment, the improved five parameters model of Lo Brano *et al.* has been used [28–30].

As concerns the thermal exchanges with surrounding environment (Figure 2), the following assumptions were made:

- The net radiative power is:

$$P = \varepsilon_{glass}\sigma\left(T_{sky}^4 - T_{glass}^4\right) + \varepsilon_{PET}\sigma\left(T_{roof}^4 - T_{PET}^4\right) \quad (1)$$

where, ε_{glass} and ε_{PET} are respectively the emissivity of the glass and PET external surfaces; σ is the Boltzmann constant; T_{sky} is the fictive sky temperature calculated with the correlation of Swinbank [31]; T_{PET} is temperature of the PET external surface of the PV panel [K]; T_{roof} is the temperature of the external surface of the roof. In the proposed algorithm, the value of T_{roof} is equal to the external air temperature T_{air} .

- The heat rate "generated" (or, more appropriately, absorbed by incident radiation and not converted into electricity) in the silicon layer is:

$$P = \tau\alpha G - \frac{V^2}{R} \quad (2)$$

where G is the solar radiation (W/m^2); V is the voltage generated by the panel; R is a pure resistive electrical load; and τα is the product of transmission coefficient of glazing and absorption coefficient of silicon.

Figure 2. Sketch of energy exchanges of PV panel with surrounding environment.

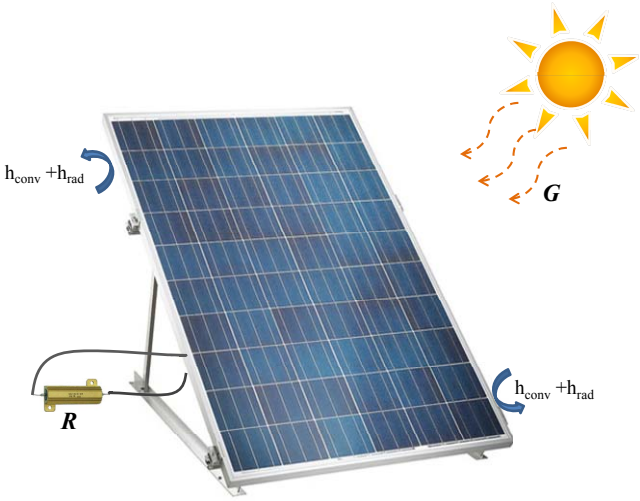

3. 1-D Thermal Model Based on Explicit Finite Difference Method

If we consider a one-dimensional approach with constant thermo-physical properties and without internal heat generation, assuming that the heat transfer is only due to conduction, the problem can be described by a system of equations involving two heat diffusion equations and an energy balance related to the PCM [25–27,32–36]:

$$\left.\begin{aligned} \frac{\partial^2 T}{\partial x^2} &= \frac{1}{\alpha_s}\frac{\partial T}{\partial t} \\ \frac{\partial^2 T}{\partial x^2} &= \frac{1}{\alpha_l}\frac{\partial T}{\partial t} \\ \lambda_s \left.\frac{\partial T}{\partial x}\right|_{x=X(t)} - \lambda_l \left.\frac{\partial T}{\partial x}\right|_{x=X(t)} &= \rho_s \cdot l \frac{\mathrm{d}X(t)}{\mathrm{d}t} \end{aligned}\right\} \quad (3)$$

where α and λ are the thermal diffusivity and the thermal conductivity respectively; the superscripts *s* and *l* refer to the solid and liquid phase; *l* is the specific solidification latent heat; and $x = X(t)$ is the time function that identifies the position of the phase change boundary [37].

The balance relating to the system of Equations (3) refers to the energy balance of a homogeneous, continuous, isotropic system in one-dimensional geometry; the application of the finite difference method requires the discretization of the system both in space and time. However, in case of phase change of the medium, it is easier to use equations that are function of enthalpy variation, thus allowing us to reduce the above system to a single equation. The following model adopts the enthalpy approach, although other methods may be used, in order to allow for a simpler implementation into an algorithm.

If we assume that T_m is the temperature of the phase change and the liquid fraction is defined as:

$$f_n = \begin{cases} 1 \; if \; T_i > T_m \\ f_n(t) \; if \; T_i = T_m \\ 0 \; if \; T_i < T_m \end{cases} \tag{4}$$

The total enthalpy *I* can be expressed as sum of the sensible component *S* and the latent component *Lf*:

$$I = S + L \cdot f \tag{5}$$

Then, rearranging the previous expressions:

$$I = S + Lf \Rightarrow \frac{\partial I}{\partial t} = \frac{\partial S}{\partial t} + L\frac{\partial f}{\partial t} \tag{6}$$

$$dS = CdT \tag{7}$$

where C is the average heat capacity of an uncompressible substance (for small temperature variations the specific heat capacity can be assumed as constant).

In this case the previous system equation can be merged in a unique expression:

$$\frac{\partial I}{\partial t} = C\frac{\partial T}{\partial t} + L\frac{\partial f}{\partial t} \tag{8}$$

In the following paragraphs the enthalpy balance is separately written for superficial and internal nodes for different initial conditions, in order to explain the dependence of phase change from the position of node.

Equation (8) allows one to assess the enthalpy balance of the domain that pertains superficial and internal nodes. The finite difference approximation of the total enthalpy can be written as:

$$\frac{\partial I_n}{\partial t} \approx \frac{I_n^{p+1} - I_n^p}{\Delta t} = \frac{S_n^{p+1} - S_n^p}{\Delta t} + L\frac{f_n^{p+1} - f_n^p}{\Delta t} \tag{9}$$

where the subscript *n* identifies the position of the examined nodal point and the superscript *p* denotes the time dependence; *p* + *1* denotes the present time while *p* denotes the previous time interval. To ensure the convergence of Equation (9) the condition should be fulfilled [38]:

$$\frac{\Delta t}{\Delta x^2} \leq \frac{\rho C}{2\lambda} \tag{10}$$

3.1. Application of Enthalpy Balance

The thickness of the control volume associated with a generic border node 0 is halved respect to the thickness of a generic internal node; hence, using the enthalpy notation of Equation (8) and assuming that on the external surface there is a generic heat flux q (that takes into account the radiative exchange with surrounding environment) and a convective heat transfer process, we can state that:

$$\frac{\partial I_n}{\partial t} \approx \frac{I_n^{p+1} - I_n^p}{\Delta t} = hA\left(T_\infty^p - T_0^p\right) + 2\frac{\bar{\lambda}_{1\to 0} A}{\Delta x}\left(T_1^p - T_0^p\right) + q^p A \tag{11}$$

where:

$$\frac{I_n^{p+1} - I_n^p}{\Delta t} = \frac{S_0^{p+1} - S_0^p}{\Delta t} + L\frac{f_0^{p+1} - f_0^p}{\Delta t} = \rho_0 c_0 A\frac{\Delta x}{2\Delta t}\left(T_0^{p+1} - T_0^p\right) + l\rho_0 A\frac{\Delta x}{2\Delta t}\left(f_0^{p+1} - f_0^p\right) \tag{12}$$

and then:

$$\rho_0 c_0\left(T_0^{p+1} - T_0^p\right) + l\rho_0\left(f_0^{p+1} - f_0^p\right) = 2h\Delta t\frac{\left(T_\infty^p - T_0^p\right)}{\Delta x} + 4\frac{\bar{\lambda}_{1\to 0}\Delta t}{\Delta x^2}\left(T_1^p - T_0^p\right) + 2q^p\frac{\Delta t}{\Delta x} \tag{13}$$

where A is the surface of the control volume (m^2); ρ_0 is the density of the control volume pertaining the superficial node 0 ($kg \cdot m^{-3}$); c_0 is the specific heat at constant pressure pertaining the superficial node 0 ($J \cdot kg^{-1} \cdot K^{-1}$); $\Delta x/2$ is the thickness of the superficial domain 0 (m); $\bar{\lambda}_{1\to 0} = \frac{\lambda_0\lambda_1}{\lambda_0 + \lambda_1}$ is a function of thermal conductivities pertaining the superficial node 0 and the internal node 1 ($W \cdot m^{-1} \cdot K^{-1}$); T_0^{p+1} is the temperature of the superficial node at the present time (K); T_0^p is the temperature of the superficial node at the past time or previous time step (K); h is the convective heat transfer coefficient ($W \cdot m^{-2} \cdot K^{-1}$) calculated with the correlation of Furushima [39]; T_∞^p is the air temperature at the past time (K); T_1^p is the temperature of the first internal node (after the superficial one) at the past time (K); q^p is the external heat flux at the past time ($W \cdot m^{-2}$); l is the specific latent heat ($J \cdot kg^{-1}$). A similar total enthalpy balance may be also written for a generic internal node, assuming the presence of a generic conductive heat flow coming from the previous and the next node.

Furthermore, the enthalpy/energy balance is written considering also the presence of the energy flow due to the absorption of solar irradiance by the silicon layer. Given the thinness of this layer, (about 0.3 mm) and the high thermal conductivity of this material, the silicon layer is considered as a virtual surface that separates the glass layer and the support material of the cells (plastic). For this purpose, the discretisation of the system is operated so that this separation surface (silicon) does not coincide with the position of any node; otherwise would be impossible to describe any extensive property pertaining this node and its domain. The energy deposition due to the absorption of solar irradiance is taken into account by considering two conductive heat flows: one that goes to the glass layer and the other that goes to the plastic layer. The paths among the point of origin of this energy deposition (the virtual surface of silicon), the glass (node n) and the plastic (node $n + 1$) layers are then equal to half of the distance between two nodes. For this reason, only in this case, the arrows do not extend between two nodes but originate from the separation surface (silicon).

Denoting by $q_{n+1\to n}$ the flow that is originated in the separation border between the nodes $n+1$ and n (Figure 3), we can write the total enthalpy balance in explicit discretized form; this method

allows to calculate the state of a system at the successive time step "$t + 1$", once calculated the state of the system at the current time "t".

Figure 3. Scheme of spatial discretization of PV-PCM system.

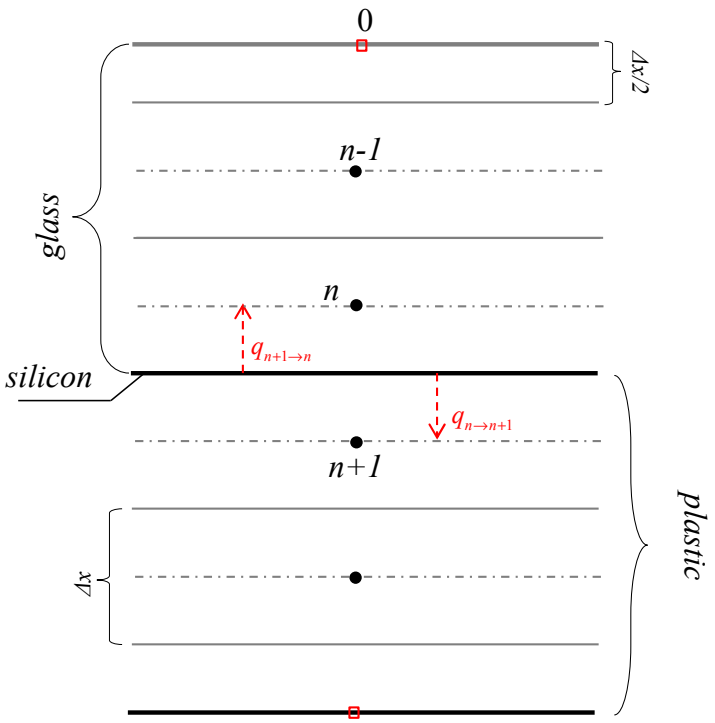

Starting from the approach followed by [40], where a simple implicit computational model for isothermal phase change was presented, the authors developed a modified algorithm based on an explicit finite difference formulation of the heat equation. The explicit approach followed by the Authors has been proved numerically stable and convergent if the Fourier number is less than 0.5 (which is our case). In contrast with the method by Zivkovic *et al.* [40], our approach is generally less numerically intensive compared with the implicit method. A forward difference at time t and a first-order central difference for the space derivative at position x was used. In order to use the method for the PV-panel system, two sets of recursive equations have been developed for two types of spatial domains: a boundary domain characterized by a length equal to $\Delta x / 2$ with a representative node placed on the surface, and an internal domain with length equal to Δx with a representative node placed in the middle. The novelty concerning the definition of a boundary domain allows us to directly consider the radiative and convective heat transfer occurring on the surface in the recursive equation. Furthermore, the presence of a generic local heat flux q is always considered to properly simulate the eventual presence of an active surface.

In the crystalline PV-PCM model such a heat flux will be not null only at one border between two consecutive nodes, where is located the surface of silicon; the flux q will be obviously null elsewhere. In the hypothesis of only conductive heat flux coming from the previous and next nodes, it is possible to write that for the n-th domain:

$$\begin{aligned}&\frac{I_n^{p+1}-I_n^p}{\Delta t}=\rho_n c_n A\frac{\Delta x}{\Delta t}\left(T_n^{p+1}-T_n^p\right)+l\rho_n A\frac{\Delta x}{\Delta t}\left(f_n^{p+1}-f_n^p\right)\\&=\frac{\overline{\lambda}_{n-1\to n}A}{\Delta x}\left(T_{n-1}^p-T_n^p\right)+\frac{\overline{\lambda}_{n\leftarrow n+1}A}{\Delta x}\left(T_{n+1}^p-T_n^p\right)+q_{n-1\to n}\frac{\lambda_n}{\lambda_{n-1}+\lambda_n}A+q_{n\leftarrow n+1}\frac{\lambda_n}{\lambda_n+\lambda_{n+1}}A\end{aligned}\tag{14}$$

and then:

$$\begin{aligned}&\rho_n c_n\left(T_n^{p+1}-T_n^p\right)+l\rho_n\left(f_n^{p+1}-f_n^p\right)\\&=\frac{\overline{\lambda}_{n-1\to n}\Delta t}{\Delta x^2}\left(T_{n-1}^p-T_n^p\right)+\frac{\overline{\lambda}_{n+1\to n}\Delta t}{\Delta x^2}\left(T_{n+1}^p-T_n^p\right)+q_{n-1\to n}\frac{\lambda_n\Delta t}{\Delta x\left(\lambda_{n-1}+\lambda_n\right)}+q_{n\leftarrow n+1}\frac{\lambda_n\Delta t}{\Delta x\left(\lambda_n+\lambda_{n+1}\right)}\end{aligned}\tag{15}$$

As already written above, the proposed model takes into account the liquid fraction neglecting the mushy phase. For the resolution of Equations (13) and (15), representing the enthalpy balance for control volumes associated with superficial and internal nodes at the time p + 1, respectively, we should distinguish four different cases:

- Case I: No phase change;
- Case II: phase change;
- Case III: Just started phase change;
- Case IV: Just ending phase change.

3.1.1. Case I: Fully Solid or Fully Liquid (No Phase Change)

$$f_n^{p+1}=f_n^p=0\ \text{ or }\ f_n^{p+1}=f_n^p=1\tag{16}$$

In this case there is not any phase change and the time variation of the liquid fraction is null. The Equations (13) and (15) can be solved by iterative method in terms of temperature:

For the superficial node:

$$T_0^{p+1}=T_0^p+2h\Delta t\frac{\left(T_\infty^p-T_0^p\right)}{\rho_0 c_0\Delta x}+4\frac{\overline{\lambda}_{1\to 0}\Delta t}{\rho_0 c_0\Delta x^2}\left(T_1^p-T_0^p\right)+2q^p\frac{\Delta t}{\rho_0 c_0\Delta x}\tag{17}$$

For internal nodes:

$$T_n^{p+1}=T_n^p+\frac{\overline{\lambda}_{n-1\to n}\Delta t}{\rho_n c_n\Delta x^2}\left(T_{n-1}^p-T_n^p\right)+\frac{\overline{\lambda}_{n+1\to n}\Delta t}{\rho_n c_n\Delta x^2}\left(T_{n+1}^p-T_n^p\right)+q_{n-1\to n}\frac{\lambda_n\Delta t}{\rho_n c_n\Delta x\left(\lambda_{n-1}+\lambda_n\right)}+q_{n\leftarrow n+1}\frac{\lambda_n\Delta t}{\rho_n c_n\Delta x\left(\lambda_n+\lambda_{n+1}\right)}\tag{18}$$

3.1.2. Case II: Phase Change

$$0<f_n^{p+1}<1\quad and\quad 0<f_n^p<1\tag{19}$$

When the phase change is occurring, it is possible to make some observations. First of all, if the phase change is isothermal, during this process the temperature is locked to the value T_m as long as the liquid fraction is between 0 and 1. Obviously, during the process the variation of sensible enthalpy is null. When the phase change is starting the superficial temperature is T_m , and the unknown value is represented by the liquid fraction. In this case it is possible to state:

$$\frac{\partial S}{\partial t} = 0 \quad and \quad T_n^p = T_n^{p+1} = T_m \tag{20}$$

In this condition the liquid fraction is:

1. For the superficial node:

$$f_0^{p+1} = f_0^p + 2h\Delta t \frac{\left(T_\infty^p - T_m\right)}{l\rho_0 \Delta x} + 4\frac{\bar{\lambda}_{1\to 0}\Delta t}{l\rho_0 \Delta x^2}\left(T_1^p - T_m\right) + 2q^p \frac{\Delta t}{l\rho_0 \Delta x} \tag{21}$$

2. For the internal nodes:

$$f_n^{p+1} = f_n^p + \frac{\bar{\lambda}_{n-1\to n}\Delta t}{l\rho_n \Delta x^2}\left(T_{n-1}^p - T_m\right) + \frac{\bar{\lambda}_{n+1\to n}\Delta t}{l\rho_n \Delta x^2}\left(T_{n+1}^p - T_m\right) + q_{n-1\to n}\frac{\lambda_n \Delta t}{l\rho_n \Delta x\left(\lambda_{n-1} + \lambda_n\right)} + q_{n\leftarrow n+1}\frac{\lambda_n \Delta t}{l\rho_n \Delta x\left(\lambda_n + \lambda_{n+1}\right)} \tag{22}$$

3.1.3. Case III: Just started Phase Change

$$T_n^{p+1} = T_m; \;\; T_n^{p+1} \neq T_n^p; \tag{23}$$

$$0 < f_n^{p+1} < 1 \quad and \quad f_n^p = 0 \text{ heat absorption } T_n^{p+1} = T_m \quad and \quad T_n^p < T_m \tag{24}$$

(just started the liquefaction)

$$0 < f_n^{p+1} < 1 \quad and \quad f_n^p = 1 \text{ heat release } T_n^{p+1} = T_m \; and \quad T_n^p > T_m \tag{25}$$

(just started the solidification)

An additional term has to be evaluated to consider the sensible heat that the control volume has adsorbed/released to pass from the initial temperature T_n^p to the phase change temperature $T_n^{p+1} = T_m$ during the examined time step. The value of *c* to be considered depends on the type of transition. If the medium is melting the value of *c* is the specific heat of liquid phase. In case of solidification, the value of *c* is the specific heat of solid phase.

3. For the superficial node:

$$f_0^{p+1} = f_0^p + 2h\Delta t \frac{\left(T_\infty^p - T_m\right)}{l\rho_0 \Delta x} + 4\frac{\bar{\lambda}_{1\to 0}\Delta t}{l\rho_0 \Delta x^2}\left(T_1^p - T_m\right) + 2q^p \frac{\Delta t}{l\rho_0 \Delta x} - \frac{c}{l}\left(T_m - T_0^p\right) \tag{26}$$

4. For the internal nodes:

$$f_n^{p+1} = f_n^p + \frac{\bar{\lambda}_{n-1\to n}\Delta t}{l\rho_n \Delta x^2}\left(T_{n-1}^p - T_m\right) + \frac{\bar{\lambda}_{n+1\to n}\Delta t}{l\rho_n \Delta x^2}\left(T_{n+1}^p - T_m\right) + q_{n-1\to n}\frac{\lambda_n \Delta t}{l\rho_n \Delta x\left(\lambda_{n-1} + \lambda_n\right)} + \\ + q_{n\leftarrow n+1}\frac{\lambda_n \Delta t}{l\rho_n \Delta x\left(\lambda_n + \lambda_{n+1}\right)} - \frac{c}{l}\left(T_m - T_n^p\right) \tag{27}$$

3.1.4. Case IV: Just Ending Phase Change

$$T_n^{p+1} \neq T_n^p; \quad T_n^p = T_m \tag{28}$$

$$0 < f_n^p < 1 \quad and \quad f_n^{p+1} = 1 \text{ heat absorption } T_n^p = T_m; \quad T_n^{p+1} > T_m \tag{29}$$

(just ending the liquefaction)

$$0 < f_n^p < 1 \quad and \quad f_n^{p+1} = 0 \text{ heat release } T_n^p = T_m; \quad T_n^{p+1} < T_m \\ \text{(just ending the solidification)} \tag{30}$$

An additional term has to be evaluated to consider the sensible heat that the control volume has adsorbed/released to pass from the initial temperature T_n^p to the phase change temperature $T_n^{p+1} = T_m$ during the examined time step.

1. For the superficial node:

$$T_0^{p+1} = T_0^p + 2h\Delta t \frac{\left(T_\infty^p - T_0^p\right)}{\rho_0 c_0 \Delta x} + 4\frac{\overline{\lambda}_{1\to 0}\Delta t}{\rho_0 c_0 \Delta x^2}\left(T_1^p - T_0^p\right) + 2q^p \frac{\Delta t}{\rho_0 c_0 \Delta x} - \frac{l}{c}\left(f_0^{p+1} - f_0^p\right) \tag{31}$$

2. For the internal nodes:

$$T_n^{p+1} = T_n^p + \frac{\overline{\lambda}_{n-1\to n}\Delta t}{\rho_n c_n \Delta x^2}\left(T_{n-1}^p - T_n^p\right) + \frac{\overline{\lambda}_{n+1\to n}\Delta t}{\rho_n c_n \Delta x^2}\left(T_{n+1}^p - T_n^p\right) + \\ + q_{n-1\to n}\frac{\lambda_n \Delta t}{\rho_n c_n \Delta x\left(\lambda_{n-1} + \lambda_n\right)} + q_{n\leftarrow n+1}\frac{\lambda_n \Delta t}{\rho_n c_n \Delta x\left(\lambda_n + \lambda_{n+1}\right)} - \frac{l}{c}\left(f_n^{p+1} - f_n^p\right) \tag{32}$$

When the phase change is just ending, the superficial temperature is again free to float; the last subtractive term in Equation (31) and (32) accounts for the necessary latent heat to end the phase changing.

Concerning the numerical method, the explicit approach followed by the authors can occasionally result in stability problems. In these cases, the response is affected by fluctuations that disrupt and eventually make the solution completely unreliable. There are several criteria that ensure the stability of the method, and in our case, in the definition of the time step and for the size of the domain, we considered the following condition: $Fo \le \frac{1}{2}; \quad Fo = \frac{\alpha \Delta t}{\left(\Delta x\right)^2}$.

4. Deployment of the Algorithm

The previous equations described above allow us to develop an algorithm for the automatic calculation using software. In order to simplify the description of the calculation procedure, the iterative equations used and solved for each time step Δt have been rewritten in the following general form: for the superficial node:

$$AT_{n-1}^p + BT_n^{p+1} + DT_{n+1}^p = C \tag{33}$$

For a stable and convergent solution in the algorithm the next steps are executed:

1. The coefficients A, B, C, D are calculated for each node taking into account the value of thermo-physical properties of the medium calculated at the previous time step:

$$\rho_n = \rho\left(T_n^p\right); \ \lambda_n = \lambda\left(T_n^p\right); c_n = c\left(T_n^p\right) \tag{34}$$

2. All nodal temperatures are calculated with an iterative approach; eventually, the values of thermo-physical properties are updated to make them coherent with the calculated thermal field. In our practical application we used only values referring with the liquid or solid phase (even because the range of temperature is enough narrow). Nevertheless, if the tabular values of each property are known, our algorithm can use them.

3. Only for PCM nodes, the phase of each domain are evaluated; possible conditions are: fully solid, fully liquid, starting of melting, phase changing, end of melting, starting of solidification, end of solidification.

4. Once calculated the conditions, a check is performed over temperatures, verifying that the correct equations were used. If one or more checks failed, the correct equations are used and all nodal temperatures are recalculated (back to step 2).

5. When phase change is starting, ending or occurring $T_n^{p+1} = T_m$, therefore the condition is:

$$\begin{cases} A_n = 0 \\ B_n = 1 \\ C_n = T_m \\ D_n = 0 \end{cases} \tag{35}$$

6. Once all nodal temperatures are calculated with right equations, liquid fraction for under transition PCM domains are calculated.

Figures 4 and 5 show the condition evaluation and liquid fraction calculation flow charts for rising temperature case:

Figure 4. Flow diagram of (**a**) temperature calculation and (**b**) liquid fraction calculation (rising temperature).

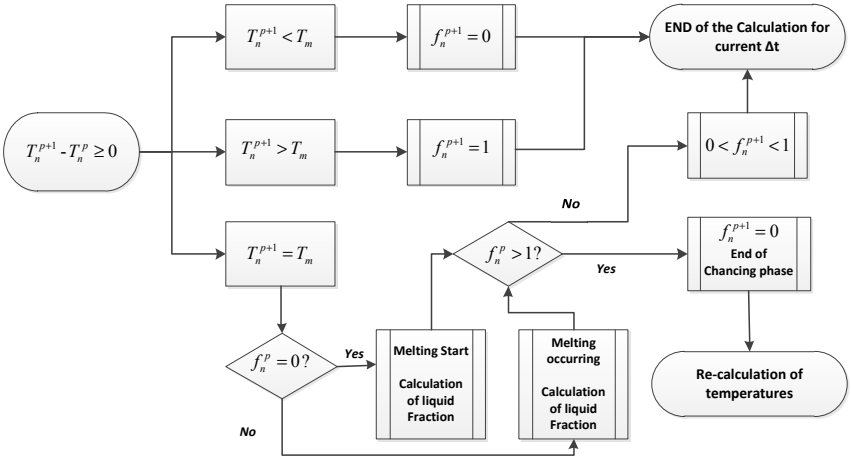

(**a**)

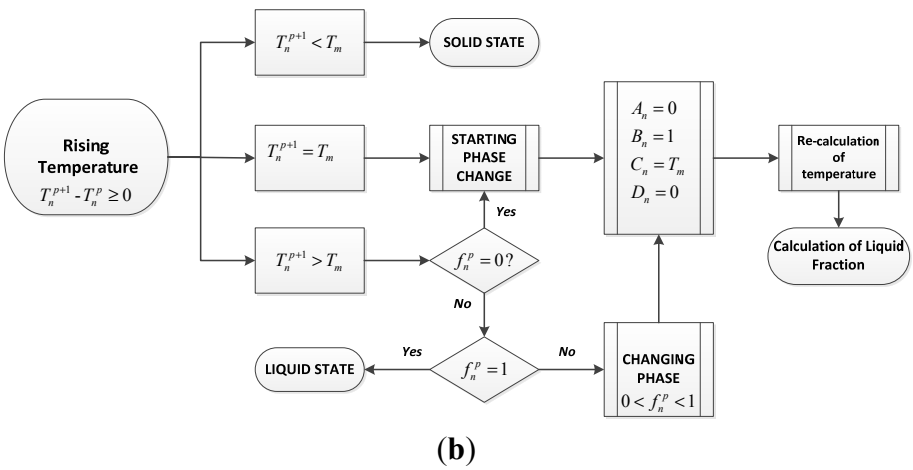

(**b**)

Figure 5. Flow diagram of (**a**) temperature calculation and (**b**) liquid fraction calculation (decreasing temperature).

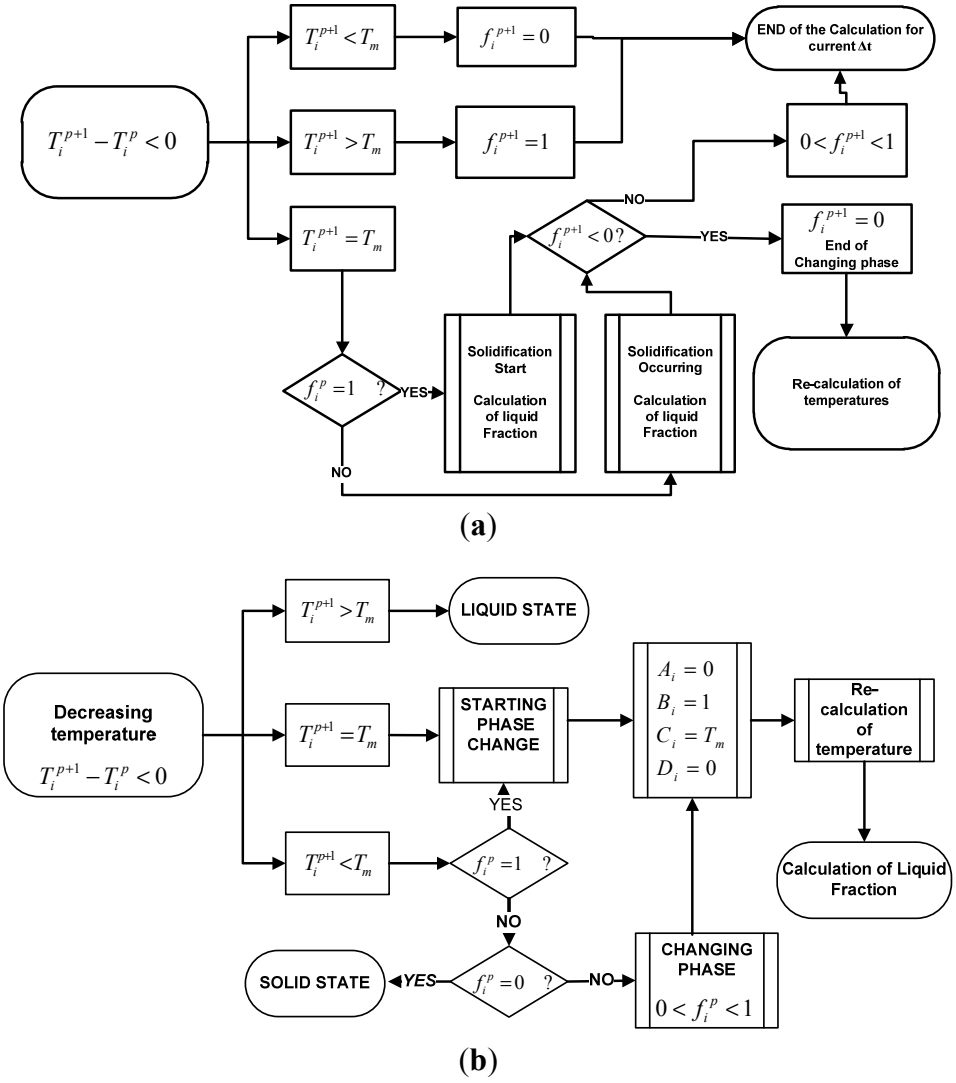

The algorithm presented was deployed in a software that uses a common programming language like VB.NET.

5. Description of Experimental Setup

In order to perform the comparison between measured and calculated data, an experimental system (Figure 6) was built up and situated on the top of the Energy Department of University of Palermo, (38°07' N, 13°22' E). The test facility consists of a silicon PV panel, a precision resistance set, a first class (ISO 9060) Delta Ohm pyrometer mod. LP PYRA 02 AV (DeltaOhm, Padova, Italy) linked to an Advantech ADAM 6024 (Advantech America, Mipitas, CA, USA) data acquisition module. A Davis Vantage PRO2 Plus Weather station (Davis Instruments Corp., Hayward, CA, USA) was used to collect the measurements of air temperature, relative humidity, wind speed and direction, horizontal global solar irradiance and atmospheric pressure.

Figure 6. Experimental set-up.

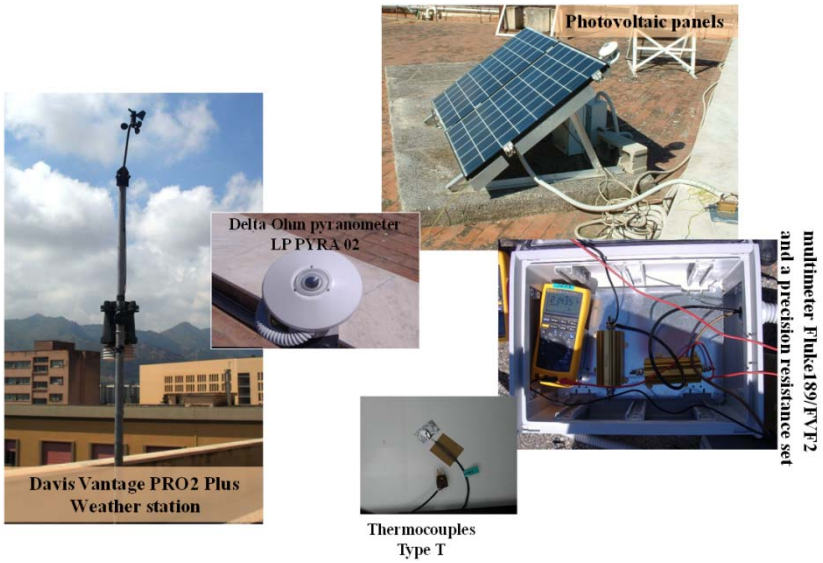

A Kyocera KC175GHT-2 PV panel (Kyocera Solar Inc., Scottsdale, AZ, USA) was coupled with a PCM layer in the bottom part using a perforated metal mesh, bolted into the frame of the panel. A galvanized hexagonal iron wire mesh with a distance of mesh holes of 54 mm and a wire thickness equal to 0.9 mm was used. The PCM was encapsulated by a double package of plastic bag (Figure 7); the thickness of the two envelopes is equal to 0.4 mm.

Figure 7. The encapsulated PCM and its installation

Concerning the heat exchange mechanism, the PCM on the upper side is in contact with the back of the photovoltaic panel; on the lower side the PCM radiatively and convectively exchanges with the external environment. The solar radiation that affects the photovoltaic panel, producing power energy and at the same time heating the panel, constitutes the flow of incoming energy into the system. No other forced heat exchange mechanism is present in the system.

The silicon temperature was measured using thermocouples (type T, copper-constantan [2]) installed into little holes (red circles in Figure 8) made in the PET rear film of the panel. All data were collected every 30 min and stored for further calculations and ex-post processing.

Figure 8. Little holes in the PET film of the PV panel to measure the temperature.

In order to measure the electrical power produced by the PV panel, the electrical circuit has been closed to precision resistances Vishay RH250, (Vishay Intertechnology Inc., Malvern, PA, USA) with a tolerance of ±1% and a temperature coefficient of ±50 ppm/°C. Since the resistances never exceeded a temperature of 150 °C, their nominal values were considered known within the precision of ±1.625% [28–30].

6. Analysis of Results

The crystalline PV-PCM system above described was monitored during the summer season, when the system is subjected to the higher solar irradiance values, because we want verify the reliability of the proposed calculation algorithm. Several numerical simulations were performed on different days and the results were compared with measured data in terms of silicon layer temperature.

As concerns the PCM, Rubitherm RT-27 packages (Rubitherm Technologies GmbH, Berlin, Germany) were used, whose chemical composition was alkane hydrocarbons with the general formula C_nH_{2n+2}. The melting points of pure paraffins depend on the number of carbon atoms, this number is between 14 and 40 and melting temperature range is between 6 and 80 °C. In the experimental application that was tested by the authors, the paraffin used was characterised by a relatively low phase transition starting temperature (26 °C), that could be interesting for the typical Sicilian summer and autumn thermal regimes. The thermo-physically characteristics of the adopted PCM are listed in Table 1.

Table 1. Thermo-physical characteristics of the PCM.

Characteristic	Value	Units
Transition phase	26–28	°C
Solid density	0.87	kg/L
Liquid density	0.75	kg/L
Heat Storage Capacity	179	kJ/kg
Specific enthalpy of phase change	1.8–2.4	J/kg
Thermal Conductivity	0.2	W/mK

Figures 9 and 10 represent the climatic conditions registered in two typical short periods of the summer season in Palermo, relating respectively with a couple of partially cloudy days and with a set of three consecutive sunny days.

Figure 9. Trends of climatic parameters in Palermo, 26–27 June 2010.

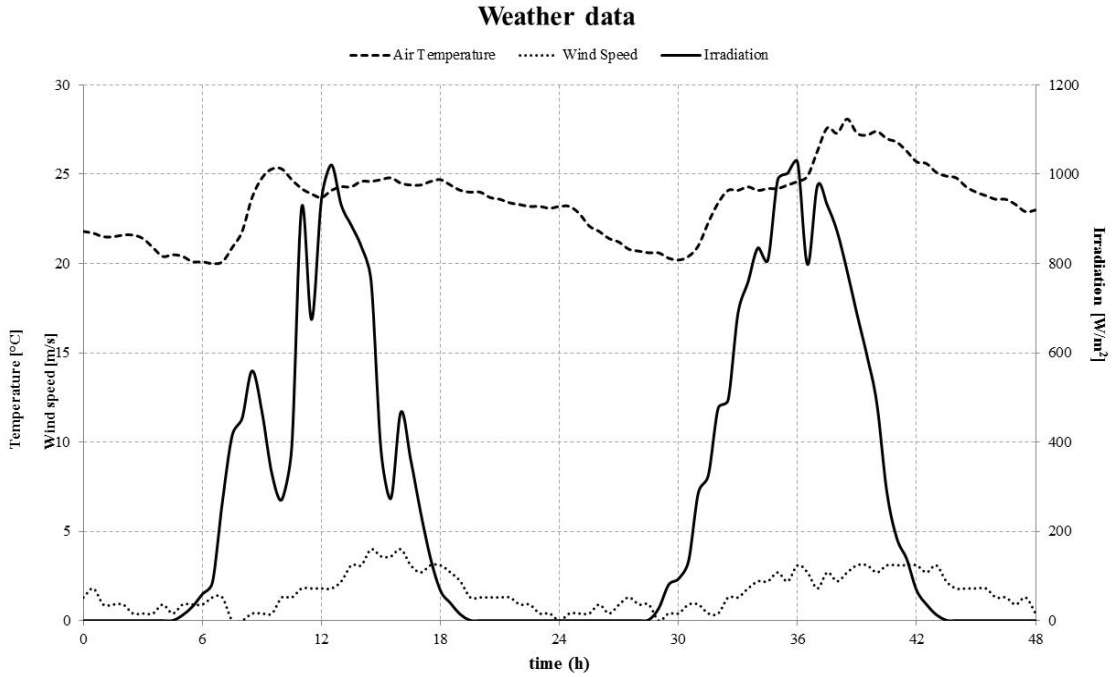

Figure 10. Trends of weather parameters in Palermo, 30 June–2 July 2010.

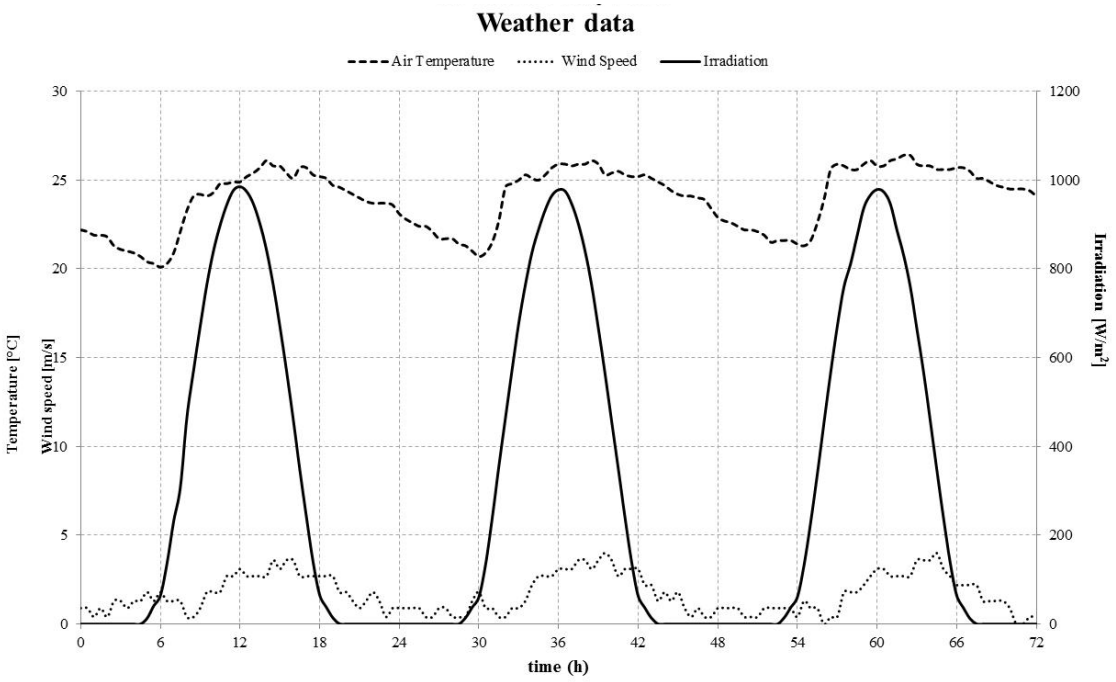

Figures 11–14 show the comparison between the measured temperatures and those calculated by the proposed algorithm. In detail Figures 11 and 13 represent the comparison of the measured and calculated temperatures of the PV system without PCM layer, the other Figures 12 and 14 show the comparison of the trend temperatures of the PV-PCM system. In both cases, the proposed algorithm good represent the operative conditions of the system.

The high temperatures measured for the PV cell and shown in Figures 12 and 14 testify to a poor performance of the paraffin as a heat storage medium. Due to the low capability of the PCM to

discharge the surplus heat during the night, (as consequence of its low thermal diffusivity) the paraffin is revealed to be efficient in cooling the panel only for few days after the installation; this result, although controversial in literature [13,41,42] has been verified experimentally in previous works.

Figure 11. Temperature trend of the measured and simulated PV system together with measured power output, in Palermo, 26–27 June 2010.

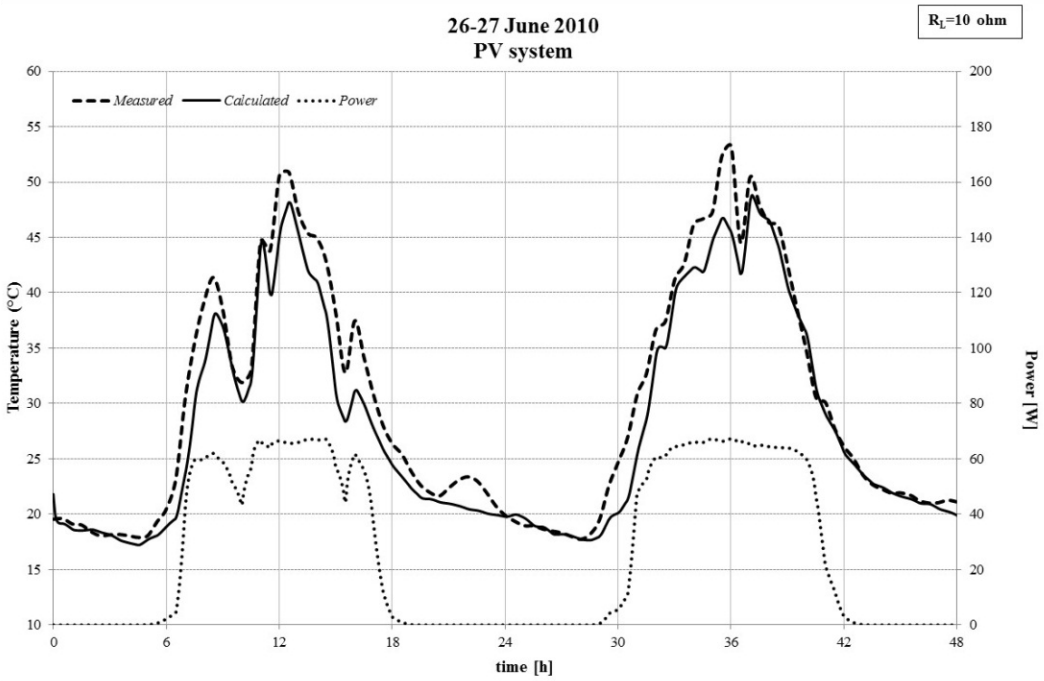

Figure 12. Temperature trend of the measured and simulated PV-PCM system together with measured power output, in Palermo, 26–27 June 2010.

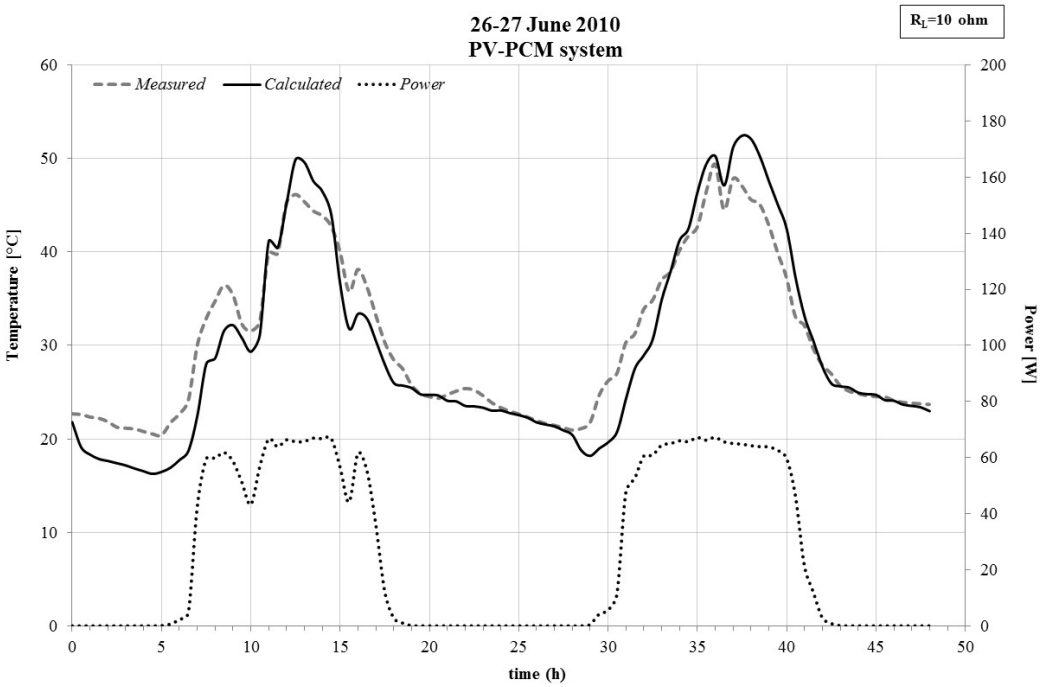

Figure 13. Temperature trend of the measured and simulated PV system, together with measured power output, in Palermo, 30 June–2 July 2010.

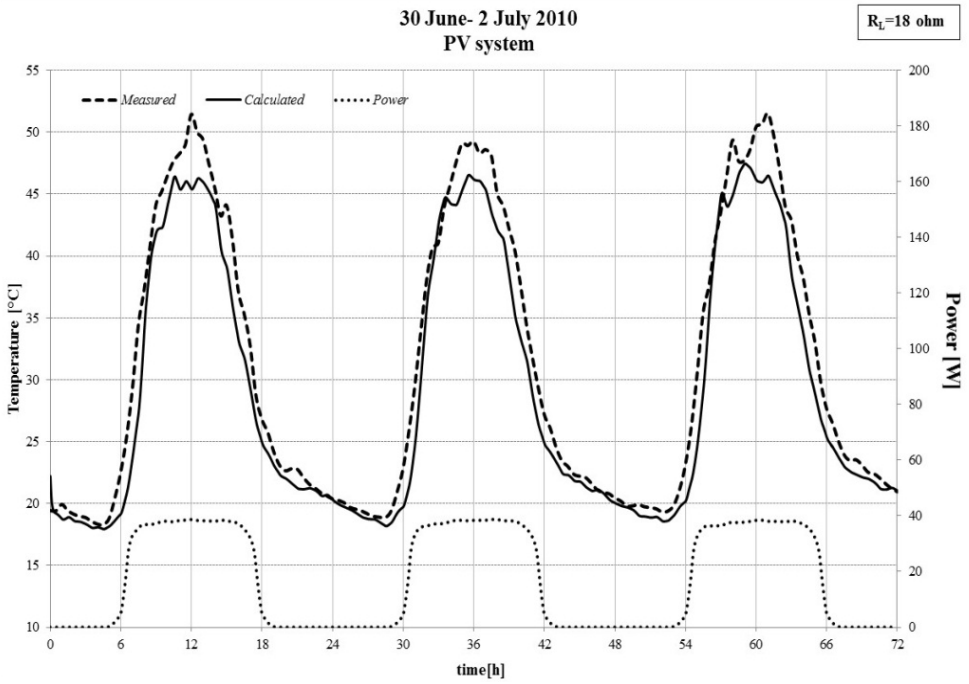

Figure 14. Temperature trend of the measured and simulated PV-PCM system together with measured power output, in Palermo, 30 June–2 July 2010.

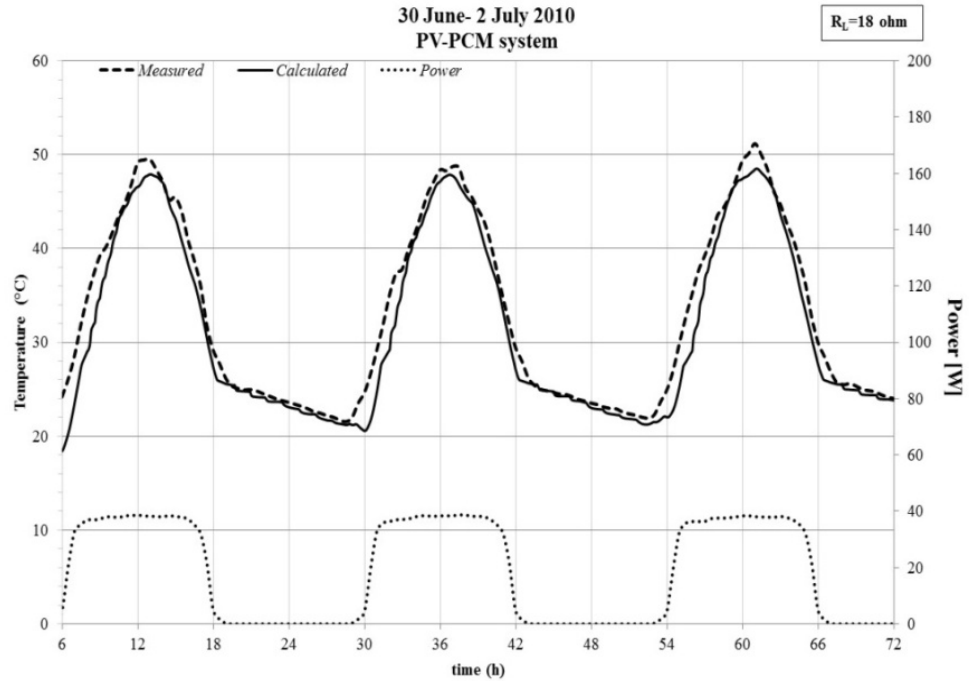

It may be observed that a flat power profile occurred during the hours with highest irradiance; this is due to the reaching of saturation conditions of the PV panel, where significant changes in solar irradiance do not induce variations in the power output. This particular operating condition was voluntarily selected for our study; in fact, under saturation conditions, the temperature of the PV panel experiences wider fluctuations being inhibited any further increase in power output delivery.

The finite differences calculation model of the PV panel coupled with a PCM thermal storage system has achieved excellent results both for sunny and partially cloudy days. The average percentage gap is calculated as $[(T_{calculated}-T_{measured})/T_{measured}]$, while the absolute value is calculated as $[\,|\,T_{calculated}-T_{measured}\,|\,/T_{measured}]$.

Looking at the graphs represented before, it is possible to see as the calculated temperature trend's is in good agreement with measured temperatures, validating the reliability of the calculation model.

The calculated temperatures at night are significantly lower than the comparable measured: this is an indication of an incorrect estimate irradiative heat exchange, which were estimated under the assumption of the sky always clear. Table 2 shows that the differences between the measured and calculated values are acceptable.

Table 2. Comparison between measured and calculated operative temperature of PV-PCM system.

Gaps		27–28 June	30 June–2 July
Operative temperature	Relative Average gap	4.85%	4.90%
	Absolute Relative Average gap	8.37%	4.92%
	Maximum negative gap	−6.43 °C	−0.11 °C
	Maximum positive gap	7.55 °C	6.01 °C

7. Conclusions

The heat exchange between the crystalline PV-PCM system and the surrounding environment is governed by several variables such as the thermo-physical properties of all the materials making up the system, the geometry, the weather conditions, the heat transfer coefficients (radiative and convective). The aim of this paper was to develop a simplified numerical model, relying upon the assumption of a one-dimensional geometry and was proposed for a PV system coupled with a PCM-based heat storage. The model is based on two sets of recursive equations that apply to two distinct types of spatial domains: internal domains with a length equal to Δx and a representative node located in the middle, and a boundary domain with halved length ($\Delta x/2$) and a representative node placed on the surface. The method assumes the phase change to be strictly isothermal and updates, at each time step, the liquid fraction of domains and the temperature of corresponding nodes. A comparison was performed between the numerical results achieved by the proposed algorithm and the experimental data obtained *in-situ* at a test facility. Despite the adoption of a simplified approach, relying upon the assumption of a one-dimensional geometry, the analysis revealed that the proposed thermal model is reliable under different climatic conditions; both in the cases of sunny and partially cloudy days; in fact, the relative average gap between calculated and measured silicon temperature remained below 5%.

Data monitored in our experimental setup have demonstrated that the dominant thermal process is that one related to the discharge of the surplus heat during the night. A better thermal contact would improve the heat transfer between the rear surface of the PV and the heat storage device. However, the main limit of this system is related to the heat transfer between the PCM heat storage and the surrounding environment. The cyclic transition of the PCM during the summer happens only one day and after the PCM remained in liquid phase. These observations thus frustrate the use of paraffin to shave the peak temperature of a photovoltaic panel and decisively disprove the results shown in other scientific works.

In order to improve the accuracy of the simulation, the authors are working on a more sophisticated calculation scheme using the Crank-Nicolson approach [43]. Although this method is more complex to implement in software, this approach should allow us to obtain a good simulation using less computation time. Finally, the presented method can be used even for other PCM configurations such as those one employed in civil structures to improve the thermal performance of buildings envelope. In addition, the model described in the paper can be effectively used in other contexts in which the PCM is uses to smooth the peak temperature due to solar radiation.

Conflicts of Interest

The authors declare no conflict of interest.

References

1. Schneider, K.; Erez, J. The effect of carbonate chemistry on calcification and photosynthesis in the hermatypic coral Acropora eurystoma. *Limnol. Oceanogr.* **2006**, *51*, 1284–1293.
2. Cardona, E.; Piacentino, A. A measurement methodology for monitoring a CHCP pilot plant for an office building. *Energy Build.* **2003**, *35*, 919–925.
3. Cellura, M.; Campanella, L.; Ciulla, G.; Guarino, F.; Lo-Brano, V.; Cesarini, D.N.; Orioli, A. The redesign of an Italian building to reach net zero energy performances: A case study of the SHC Task 40—ECBCS Annex 52. *ASHRAE Trans.* **2011**, *117*, 331–339.
4. International Energy Agency. *World Energy Outlook 2011*; Paris OECD International Energy Agency: Paris, France, 2011.
5. Ciulla, G.; Lo Brano, V.; Marvuglia, A.; Orioli, A. A Photovoltaic Panel Coupled with a Phase Changing Material Heat Storage System in Hot Climates. In Proceeding of the 25th International Conference on Passive and Low Energy Architecture: Towards Zero Energy Building, PLEA 2008, Dublin, Ireland, 22 October 2008.
6. Lo Brano, V.; Orioli, A.; Ciulla, G.; Culotta, S. Quality of wind speed fitting distributions for the urban area of Palermo, Italy. *Renew. Energy* **2011**, *36*, 1026–1039.
7. Lopes, A.; Saraiva, J.; Alcoforado, M.J. Urban boundary layer wind speed reduction in summer due to urban growth and environmental consequences in Lisbon. *Environ. Model. Softw.* **2011**, *26*, 241–243.
8. Memon, R.A.; Leung, D.Y.C.; Liu, C.H. Effects of building aspect ratio and wind speed on air temperatures in urban-like street canyons. *Build. Environ.* **2010**, *45*, 176–188.
9. Mirzaei, P.A.; Carmeliet, J. Influence of the underneath cavity on buoyant-forced cooling of the integrated photovoltaic panels in building roof: A thermography study. *Prog. Photovolt. Res. Appl.* **2013**, doi:10.1002/pip.2390.
10. Corbin, C.D.; Zhai, Z.J. Experimental and numerical investigation on thermal and electrical performance of a building integrated photovoltaic thermal collector system. *Energy Build.* **2010**, *42*, 76–82.
11. Tyag, V.; Buddhi, D. PCM thermal storage in buildings: A state of art. *Renew. Sustain. Energy Rev.* **2007**, *11*, 1146–1166.

12. Halawa, E.; Bruno, F.; Saman, W. Numerical analysis of a PCM thermal storage system with varying wall temperature. *Energy Convers. Manag.* **2005**, *46*, 2592–2604.
13. Liu, H.; Awbi, H.B. Performance of phase change material boards under natural convection. *Build. Environ.* **2009**, *44*, 1788–1793.
14. Zhang, M.; Medina, M.A.; King, J.B. Development of a thermally enhanced frame wall with phase-change materials for on-peak air conditioning demand reduction and energy savings in residential buildings. *Int. J. Energy Res.* **2005**, *29*, 795–809.
15. Zhou, D.; Zhao, C.Y.; Tian, Y. Review on thermal energy storage with phase change materials (PCMs) in building applications. *Appl. Energy* **2012**, *92*, 593–605.
16. Izquierdo-Barrientos, M.A.; Belmonte, J.F.; Rodríguez-Sánchez, D.; Molina, A.E.; Almendros-Ibáñez, J.A. A numerical study of external building walls containing phase change materials (PCM). *Appl. Therm. Eng.* **2012**, *47*, 73–85.
17. Huang, M.J.; Eames, P.C.; Norton, B. Thermal regulation of building-integrated photovoltaic using phase change materials. *Int. J. Heat Mass Transf.* **2004**, *47*, 2715–2733.
18. Jeon, J.; Jeong, S.G.; Lee, J.H.; Seo, J.; Kim, S. High thermal performance composite PCMs loading *x*GnP for application to building using radiant floor heating system. *Solar Energy Mater. Solar Cells* **2012**, *101*, 51–56.
19. Chintakrinda, K.; Weinstein, R.D.; Fleischer, A.S. A direct comparison of three different material enhancement methods on the transient thermal response of paraffin phase change material exposed to high heat fluxes. *Int. J. Therm. Sci.* **2011**, *50*, 1639–1647.
20. Huang, M.J.; Eames, P.C.; Norton, B. Phase change materials for limiting temperature rise in building integrated photovoltaics. *Solar Energy* **2006**, *80*, 1121–1130.
21. Hasan, A.; McCormack, S.J.; Huang, M.J.; Norton, B. Evaluation of phase change materials for thermal regulation enhancement of building integrated photovoltaics. *Solar Energy* **2010**, *84*, 1601–1612.
22. Maiti, S.; Banerjee, S.; Vyas, K.; Patel, P.; Ghosh, P.K. Self-regulation of photovoltaic module temperature in V-trough using a metal-wax composite phase change matrix. *Solar Energy* **2011**, *85*, 1805–1816.
23. Weinlaeder, H.; Koerner, W.; Heidenfelder, M. Monitoring results of an interior sun protection system with integrated latent heat storage. *Energy Build.* **2011**, *43*, 2468–2475.
24. Ho, C.J.; Tanuwijava, A.O.; Lai, C.M. Thermal and electrical performance of a BIPV integrated with a microencapsulated phase change material layer. *Energy Build.* **2012**, *50*, 331–338.
25. Pascal, B.; Eclache, P.; Kuznik, F. Phase-change materials to improve solar panel's performance. *Energy Build.* **2013**, *62*, 59–67.
26. Ciulla, G.; Lo Brano, V.; Messineo, A; Peri, G. A numerical solution that determines the temperature field inside phase change materials: Application in buildings. *J. Civ. Eng. Manag.* **2013**, *19*, 518–528.
27. Huang, M.J.; Eames, P.C.; Norton, B. Comparison of a small-scale 3D PCM thermal control model with a validated 2D PCM thermal control model. *Solar Energy Mater. Solar Cells* **2006**, *90*, 1961–1972.
28. Lo Brano, V.; Orioli, A.; Ciulla, G. On the experimental validation of an improved five-parameter model for silicon photovoltaic modules. *Solar Energy Mater. Solar Cells* **2012**, *105*, 27–39.

29. Ciulla, G.; Lo Brano, V.; Moreci, E. Forecasting the cell temperature of PV modules with an adaptive system. *Int. J. Photoenergy* **2013**, doi:10.1155/2013/192854.
30. Lo Brano, V.; Ciulla, G. An efficient analytical approach for obtaining a five parameters model of photovoltaic modules using only reference data. *Appl. Energy* **2013**, *111*, 894–903.
31. Swinbank, W.C. Long-wave radiation from clear skies. *Q. J. R. Metereol. Soc.* **1963**, *89*, 339–348.
32. Mirzaei, P.A.; Haghighat, F. Modeling of phase change materials for applications in whole building simulation. *Renew. Sustain. Energy Rev.* **2012**, *16*, 5355–5362.
33. Fan, L.W.; Khodadadi, J.M. Thermal conductivity enhancement of phase change materials for thermal energy storage: A review. *Renew. Sustain. Energy Rev.* **2011**, *15*, 24–46.
34. Voller, V.R.; Cross, M. Accurate solutions of moving boundary problems using enthalpy method. *Int. J. Heat Mass Transf.* **1981**, *24*, 545–556.
35. Voller, V.R. A heat balance integral method based on an enthalpy formulation. *Int. J. Heat Mass Transf.* **1987**, *30*, 604–607.
36. Voller, V.R. Fast implicit finite-difference method for the analysis of phase change problem. *Numer. Heat Transf.* **1990**, *17*, 155–169.
37. Lamberg, P.; Lehtiniemi, R.; Henell, A.M. Numerical and experimental investigation of melting and freezing processes in phase change material storage. *Int. J. Therm. Sci.* **2004**, *43*, 277–287.
38. Incropera, F.P.; de Witt, D.P. *Fundamentals of Heat and Mass Transfer*, 5th ed.; John Wiley & Sons: New York, NY, USA, 2002.
39. Furushima, K.; Nawata, Y.; Sadatomi, M. Prediction of Photovoltaic (PV) Power Output Considering Weather Effects. In Proceedings of the ASME International Solar Energy Conference, Denver, CO, USA, 8–13 July 2006; pp. 7–13.
40. Zivkovic, B.; Fujii, I. Analysis of isothermal phase change of phase change material within rectangular and cylindrical containers. *Solar Energy* **2001**, *70*, 51–61.
41. Ciulla, G. Un Modello di Simulazione del Comportamento Termico ed Elettrico di Pannelli Fotovoltaici Piani; Miglioramento Della Resa Energetica per mezzo di Materiali a Cambiamento di Fase (in Italian). Ph.D. Thesis, University of Palermo, Palermo, Italy, February 2009.
42. Saitta, M. Materiali a Cambiamento di Fase Accoppiati a Moduli Fotovoltaici: Un'analisi Numerica (in Italian). Master's Thesis, University of Palermo, Palermo, Italy, July 2010.
43. Crank, J.; Nicolson, P. A Practical Method for Numerical Evaluation of Solutions of Partial Differential Equations of the Heat-Conduction Type. In Mathematical Proceedings of the Cambridge Philosophical Society; Cambridge University Press: Cambridge, UK, 1947; Volume 43, pp. 50–67.